Solid-State Structures of Primary Long-Chain Alkylamine Borane Adducts – Synthesis, Properties and Computational Analysis

Kevin Turani-I-Belloto, María-José Valero-Pedraza, Eddy Petit, Rodica Chiriac, François Toche, Dominique Granier, Pascal G Yot, Johan G Alauzun, Umit B Demirci

ChemistrySelect

Research Article
doi.org/10.1002/slct.202203533

Chemistry Europe
European Chemical Societies Publishing

www.chemistryselect.org

Solid-State Structures of Primary Long-Chain Alkylamine Borane Adducts – Synthesis, Properties and Computational Analysis

Kevin Turani-I-Belloto,[a] María-José Valero-Pedraza,[a] Eddy Petit,[a] Rodica Chiriac,[b] François Toche,[b] Dominique Granier,[c] Pascal G. Yot,[c] Johan G. Alauzun,[c] and Umit B. Demirci*[a]

Two new members of the amine boranes family are hexadecylamine borane $C_{16}H_{33}NH_2BH_3$ (C16AB) and octadecylamine borane $C_{18}H_{35}NH_2BH_3$ (C18AB). They are easily synthesized by reaction of the corresponding amines with borane dimethyl sulfide. Both are white solids; they are crystalline and isostructural (monoclinic, s.g. $P2_1/a$ (No. 14)). Their successful synthesis has been verified by molecular (FTIR, Raman, NMR) and structural analyses as well as computational calculations (e.g. Mulliken charges). These analyses have also pointed out the existence of dihydrogen bonds between $H^{\delta+}$ of NH_2 of one molecule and $H^{\delta-}$ of BH_3 of another molecule. The thermal stability of C16AB and C18AB was studied. Both solids melts at 70–80 °C; between 100 and ca. 210 °C they dehydrogenate while releasing 1.1-1.4 wt% of pure H_2; and, above 210 °C, they decompose in high extent. All of these findings may open the way to future works on molecular self-assembly, synthesis of advanced materials and hydrogen storage. This is discussed hereafter.

Introduction

Amine borane adducts (ABA) are old molecules with new interest.[1] A typical representative is ammonia borane NH_3BH_3 (AB). It is the fully hydrogenated ABA. It was discovered in the 1950s and was re-discovered in the late 1990s owing to its high potential for solid-state hydrogen storage.[2] In a context where energy is a hot topic, AB has thus been extensively investigated, giving way to other ABAs for the same application.[3,4] Yet, the use of ABAs goes beyond the aforementioned application.[5] ABAs have also been developed to be used as borylation agents,[6] hydroboration reagents,[7] radical initiators,[8] reducing agents,[9] hydrogenation reagents,[10] hydrogenation catalysts,[11] monomers of BNH polymers,[12] and additives for hydrocarbons combustion.[13] New ABAs are yet to be discovered, as for the recently-synthesized catharanthine borane.[14]

AB is often compared to ethane CH_3CH_3 because they are isoelectronic and have similar molecular structures.[15] Notwithstanding these two features, AB and ethane are much different in terms of physicochemical properties, because the B–N bond of the former is dative and polar whereas the C–C bond of the latter is covalent and apolar. The impact of this is considerable. First, AB is solid at ambient conditions whereas ethane is gaseous. Second, the hydrogens of the NH_3 group are protic ($H^{\delta+}$) and those of the BH_3 group are hydridic ($H^{\delta-}$), whereas the hydrogens of the CH_3 groups are neutral ($H^{\delta\sim0}$). Third, AB is unstable in the presence of protons or when heated above 80 °C, whereas ethane is stable in similar conditions.[2]

More broadly, the aforementioned similarities and differences are also true for primary alkylamine borane adducts $C_nH_{2n+1}NH_2BH_3$ (C_nNBH_{2n+6}; AABA) and *n*-alkanes C_mH_{2m+2} (with $m = n + 2$; resulting in C_nCCH_{2n+6}). They are also isoelectronic. For instance, we recently reported on an AABA where n is equal to 12.[16] This AABA, dodecylamine borane $C_{12}H_{25}NH_2BH_3$, is solid at ambient conditions, and it decomposes when heated above 80 °C. Contrariwise, dodecane $C_{12}H_{26}$ is liquid at ambient conditions, and it is stable when heated at 80-120 °C.[17]

The presence of $H^{\delta+}$ and $H^{\delta-}$ in ABAs allows the existence of intermolecular dihydrogen $H^{\delta+}\cdots H^{\delta-}$ bonds (DHBs).[18] Such bonds are stronger than the intermolecular van der Waals interactions existing between two $H^{\delta\sim0}$ of two alkane molecules. The consequence is that the DHBs stabilize the solid-state of both AB and dodecylamine borane. Additionally, DHBs play an important role in stabilizing or destabilizing an ABA to release pure H_2 at low temperature,[4] in generating reactive intermediates as for diammoniate of diborane $[(NH_3)_2BH_2]^+$

[a] *Dr. K. Turani-I-Belloto, M.-J. Valero-Pedraza, E. Petit, Prof. U. B. Demirci*
Institut Europeen des Membranes, IEM – UMR 5635
Universite de Montpellier, ENSCM, CNRS
34090 Montpellier, France
E-mail: umit.demirci@umontpellier.fr
[b] *R. Chiriac, F. Toche*
Laboratoire des Multimateriaux et Interfaces
UMR CNRS 5615, Univ Lyon 1
Université Claude Bernard Lyon 1,
F-69622 Villeurbanne, France
[c] *D. Granier, Dr. P. G. Yot, Dr. J. G. Alauzun*
Institut Charles Gerhardt,
Univ. Montpellier, CNRS, ENSCM
Montpellier, France

Supporting information for this article is available on the WWW under https://doi.org/10.1002/slct.202203533

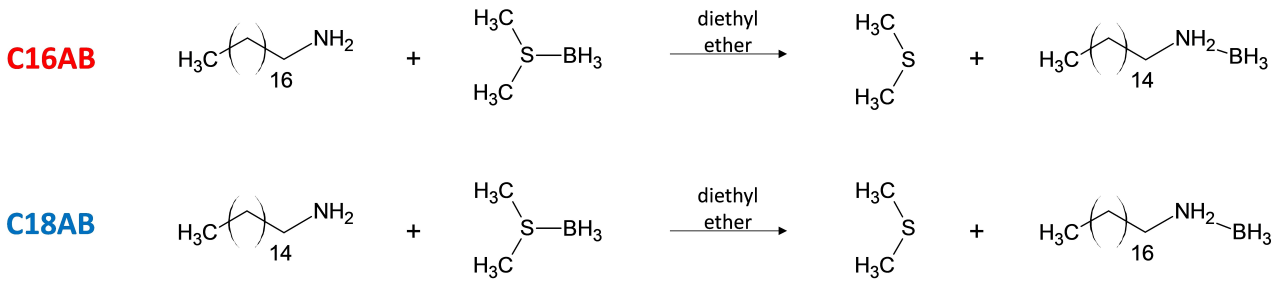

Scheme 1. Synthesis of C16AB as hexadecylamine borane, and of C18AB as octadecylamine borane, in diethyl ether.

$[BH_4]^-$ forming by $H^{\delta-}$ transfer from one AB molecule to another one,[19] in designing derivatives where a borohydride and ammonia are combined,[20] and in producing BNH polymeric structures by dehydrocoupling of ABA precursors.[21] To paraphrase Chen et al.,[18] dihydrogen $H^{\delta+}\cdots H^{\delta-}$ bonds have been less studied than the conventional hydrogen bonds, and they could be further investigated in order to explore applications such as molecular recognition, crystal engineering, molecular self-assembly, and synthesis of new advanced materials.

Our recent works have to be seen within the context mentioned above. In a previous work, we reported on the synthesis and full characterizations of six primary AABAs, i.e. $C_nH_{2n+1}NH_2BH_3$ with n equal to 4, 6, 8, 10, 12 and 14; for brevity, they are denoted C4AB, C6AB, C8AB, C10AB, C12AB and C14AB.[16] The first two are oily liquids and the other ones, which have never been synthesized before, are crystalline solids. In this work, we synthesized two new, primary long-chain AABA, such as hexadecylamine borane $C_{16}H_{33}NH_2BH_3$ and octadecylamine borane $C_{18}H_{35}NH_2BH_3$; for brevity and homogeneity, they are denoted C16AB and C18AB (Scheme 1). Both are crystalline solids. They were properly and fully characterized, and they were computationally studied. Our work has a twofold objective: gaining better understanding on AABAs and on their DHBs; and, developing AABAs like C16AB that, afterwards, could be used as surfactant for molecular self-assembly and synthesis of advanced materials.

Results and Discussion

Preliminary remarks

The two AABAs are synthesized by Lewis acid-base reaction of hexadecylamine or octadecylamine with borane dimethyl sulfide (Scheme 1) in diethyl ether. The reactions are exothermic. Boiling of diethyl ether was even observed when the borane reactant was too quickly added to the amine solution. To limit an exothermicity-induced heating of the solution, a dropwise addition was performed. We determined the enthalpy of reaction by Calvet calorimetry (Figure S1). The enthalpies are −59.4 and −69.7 kJ mol^{-1} for C16AB and C18AB. This confirms the exothermic nature of the reaction.

At ambient temperature, both C16AB and C18AB are powdery solids (yields >95%; purity ≥98% and ≥95%). They are thus easy to extract (the solvent and the dimethyl sulfide product being vacuum distillated).

Molecular analyses

C16AB was analyzed by FTIR spectroscopy while the spectrum was computationally predicted (Figure 1). The spectrum shows

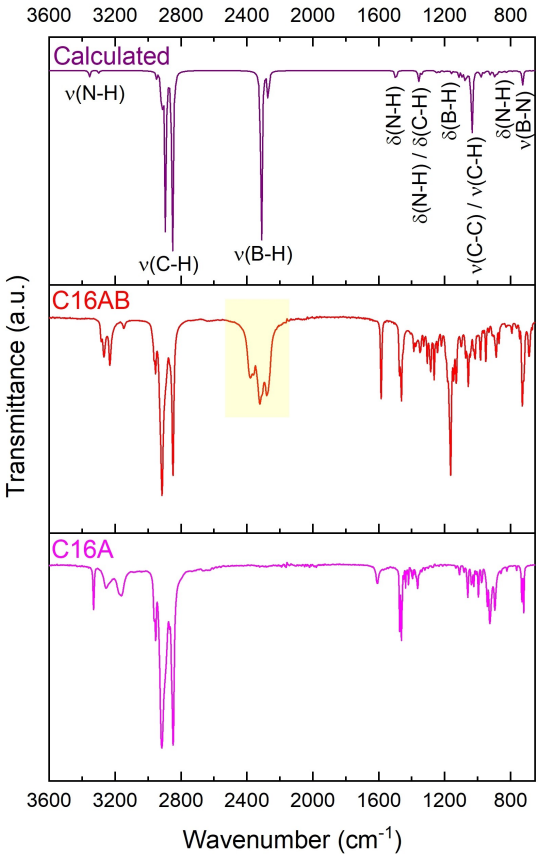

Figure 1. FTIR spectra of C16AB and of the starting amine $C_{16}H_{33}NH_2$ denoted C16 A. The predicted (calculated) spectrum is shown for comparison. The bands are attributed to the corresponding vibration modes.

N–H (3400–3100 cm^{-1}), C–H (3050–2750 cm^{-1}), and B–H (2500–2100 cm^{-1}) stretching bands due to the NH_2, $CH_3(CH_2)_{17}$, and BH_3 groups.[22] The spectrum of C16AB was compared to that of the starting amine. On one hand, the C–H stretching bands are similar. On the other hand, there are differences in the N–H stretching bands. The spectrum of the amine shows three N–H bands (3330, 3257 and 3162 cm^{-1}); that of C_{16}AB shows also the three bands but they are red shifted (3268, 3234 and 3147 cm^{-1}). This indicates a change in the N–H bond strength, which is in line with the formation of the polarized B–N bond and the concomitant occurrence of DHBs. The spectra are complex over the wavenumber range 1200–650 cm^{-1}. There are many bands caused by vibrations of C–H, C–C, B–H, C–N, and B–N. For instance, the spectrum of C16AB shows an additional band due to the stretching mode of the B–N bond at about 690 cm^{-1}. The experimental and calculated Raman spectra of C16AB (Figure S2) corroborate these observations. It can thus be concluded that C16AB was successfully produced.

C16AB in CD_3CN solution was analyzed by NMR spectroscopy. The ^{1}HNMR spectrum (Figure S3) shows six signals that confirm the molecular structure of the AABA: namely, a large multiplet of low intensity between 0.5 and 2 ppm due to the 3 H of BH_3; a triplet at 0.91 ppm due to the 3 H of CH_3; a broad signal at 1.31 ppm due to the CH_2 groups between CH_3 and the beta CH_2; a multiplet at 1.56 ppm due to the 2 H of CH_2CH$_2$N; a quintet at 2.61 ppm due to the 2 H of CH_2N; a broad singlet at 3.91 ppm due to the 2 H of NH_2. This was further confirmed by simulation of the chemical shifts (Figure S4). The ^{1}HNMR data were used to determine the purity of C16AB; it is ≥98%. The ^{11}BNMR spectrum of C16AB (Figure 2) shows a quartet at −19.65 ppm of normalized intensity 1:2.5:2.5:1 and with a coupling constant $^1J_{B-H}$ of 95.3 Hz. This is characteristic of a NBH$_3$ environment.[23]

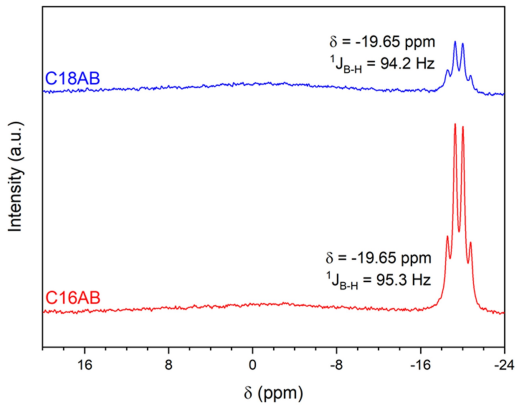

Figure 2. ^{11}BNMR spectra of C16AB and C18AB (dissolved in CD_3CN). The chemical shift and the coupling constant of the quartets are given.

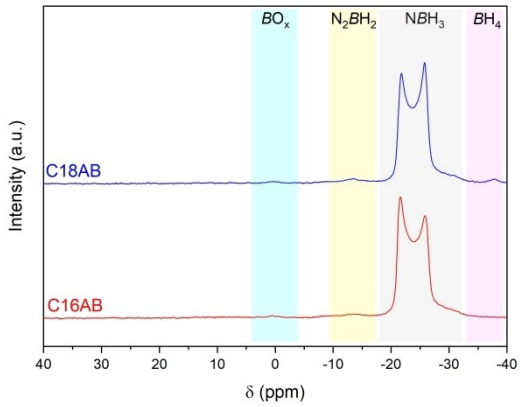

Figure 3. ^{11}B MASNMR of C16AB and C18AB. The signals are assigned.

As C16AB is solid at ambient temperature, it was also analyzed by ^{11}B MASNMR (Figure 3). The spectrum shows a two-horned peak centered at −23.8 ppm, typical of a NBH$_3$ environment.[24] Our calculations predicted a shift of −24.7 ppm, which is consistent with the experimental shift. When the baseline is scrutinized, two signals with very low intensity (at −13.7 and 0 ppm) can be observed. The signals at negative chemical shift can be attributed to N_2BH_2 environment. It suggests a slight evolution of C16AB (dehydropolymerization),[25] likely to be as follows:

$$2C_{16}H_{33}NH_2BH_3 \rightarrow C_{16}H_{33}NH_2BH_2{-}NH_2(C_{16}H_{33})BH_3 \quad (1)$$

The signal at 0 ppm is generally indicative of B–O bonds, probably due to moist air contamination (when transferred to the spectrometer located in another building) and subsequent hydrolysis.[16]

With respect to C18AB, the FTIR (Figure S5), Raman (Figure S6), ^{1}HNMR (Figure S7), simulated ^{1}HNMR (Figure S8) and ^{11}BNMR (Figure 2) spectra are much comparable to those of C16AB. They all allow drawing the same conclusion, that is, the successful production of C18AB. Based on the ^{1}HNMR data, the purity of C18AB was calculated as ≥95%. C18AB was also analyzed by ^{11}B MASNMR (Figure 3). The two-horned peak centered at −23.7 ppm (and computationally predicted at −24.7 ppm) confirms the presence of a NBH$_3$ environment. The baseline shows three signals of low intensity, at −13.8 (N_2BH_2), 0 ppm (BO_x) and −37.8 ppm; the last one is attributed to a BH_4 environment.[25] The concomitant presence of the environments N_2BH_2 and BH_4 may indicate the formation of an ionic dimer of C18AB:

$$2C_{18}H_{37}NH_2BH_3 \rightarrow [(C_{18}H_{37}NH_2)_2BH_2]^+[BH_4]^- \quad (2)$$

This species would form by transfer of H^- from BH_3 of one C18AB molecule to BH_3 of another one, and this would be mediated by the DHBs.[19]

Structural analyses

C16AB and C18AB are crystalline (Figure 4 and Figures S9–S10). Regardless of the alkyl chain length, both solids crystallize in the monoclinic system, and as it has been found in a previous work with the solids C_{10}AB, C_{12}AB and C_{14}AB.[16] The space group

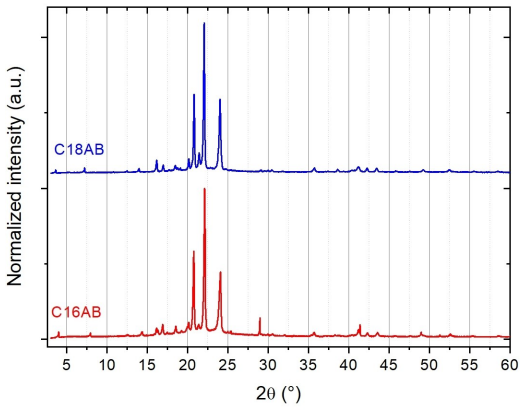

Figure 4. Powder X-ray diffraction patterns obtained for C16AB and C18AB in the range 2.5–50° (λ = 1.54059 Å).

is $P2_1/a$ (No. 14) for both C16AB and C18AB. In other words, the increase in the alkyl chains in C16AB and C18AB gives no difference into the symmetry: the solids are isostructural; and, the lattice parameters (Table 1) follow the same trends (as found in our previous work), that is, the b and c unit-cell parameters are close to each other and consistent to the values obtained for the solids based on shorter alkyl chains,[16] and the a unit-cell parameter increases with the number of carbons such as ca. 4.5 Å per carbon added.

Table 1. Space group, number of asymmetric unit (Z), unit cell parameters (a, b, c, β), and unit cell volume, for solid-state C16AB and C18AB after refinement of the powder diffraction patterns.

CxAB	C16AB	C18AB
Formulae	$C_{16}H_{33}NH_2BH_3$ $B_1N_1C_{16}H_{38}$	$C_{18}H_{37}NH_2BH_3$ $B_1N_1C_{18}H_{42}$
Space group	*P21/a*	*P21/a*
Z	4	4
a (Å)	44.655(6)	49.415(5)
b (Å)	7.3980(5)	7.4075(4)
c (Å)	5.4963(5)	5.5144(4)
β (°)	94.310(10)	96.574(7)
Volume (Å^3)	1810.6(3)	2005.2(3)
Density	0.9366	0.9386
Mw (g mol^{-1})	255.3	283.4
GoF	2.95	2.77
Rp (%)	8.34	9.60
wRp (%)	11.99	13.49
Robs (%)	13.85	13.32
wR(obs) (%)	14.91	13.30
R(all) (%)	14.7	13.52
wR(all) (%)	14.78	13.37

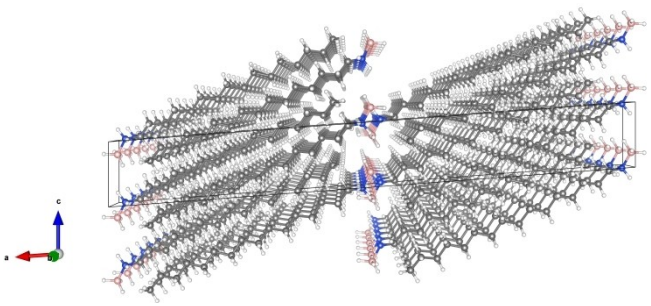

Figure 5. Crystal structure of C16AB. The H, B, N and C atoms are represented by white, pink, blue and dark grey spheres, respectively.

The structural models do not present noticeable difference in comparison to C6AB, C8AB, C10AB and C12AB.[16] The chains are aligned together and are diagonal into plane parallel to the (040) plane giving layers to form a close-packed arrangement (Figure 5 and Figures S11-S12). All the intermolecular distances (Table S1) have been measured for the two solids. The number of carbons affects the shortest C-to-C distance increasing form from 4 to 4.1 Å (while 4–4.3 Å for C6AB to C12AB). At the same time, the B-to-C distance is close to 4 Å and is consistent with the ones determined for C6AB to C12AB. However, the N-to-C distances are strongly affected, with values of 4.4 and 4.65 Å (while 4.44 and 5 Å for C6AB to C12AB). The C-to-C distances into the planes (040) as defined by the aligned chains are close to 4.49 Å (versus 4.14 and 4.40 Å for C6AB to C12AB). The antiparallel NH_2BH_3 dimeric configuration, that is, NH_2 of one molecule facing BH_3 of another molecule along the b axis (and the *bc* plane), gives intermolecular B-to-N distances between 4.05 and 4.3 Å. Such a configuration is typical of the occurrence of DHBs.

Electronic analyses

The C16AB and C18AB molecules were studied by DFT calculations. The total energy of each was calculated. The total energy of the C16AB molecule is −712.45 Hartree. With respect to the C18AB molecule that has two more CH_2 groups (and the corresponding molecular orbitals), the absolute value of the total energy is higher; the total energy is −791.10 Hartree.

The Mulliken charges were extracted (Figures S13–S14). The charges for both the C16AB and C18AB molecules are as follows: −0.376 for N, 0.031–0.034 for B, 0.286–0.287 for H of the N–H bonds, and −0.1 for H of the B–H bonds. The charges of the hydrogens confirm the presence of $H^{\delta+}$ and $H^{\delta-}$, and thus the occurrence of DHBs. It is worth mentioning the negative charges of the alpha (−0.547 and −0.490 respectively) and beta (−0.256 and −0.195 respectively) carbons for the C16AB and C18AB molecules. These differences of charges are also illustrated by the mapped electrostatic potentials (Figures S15–S16). In addition, the distribution of the highest occupied molecular orbital (HOMO) and that of the lowest unoccupied molecular orbital (LUMO), over each of the molecules, were plotted (Figure 6). For both the C16AB and C18AB molecules, the HOMO is mainly localized on the C–C–N bonds, and the LUMO mainly comes for the BH_3 group and is slightly delocalized to the adjacent N–C–C–C–C bonds. All of these observations are in line with the known reactivity of the NH_2BH_3 group of the ABAs,[1–4] and they also show that the bond between N and alpha C and that between alpha C and beta C are likely to be reactive.

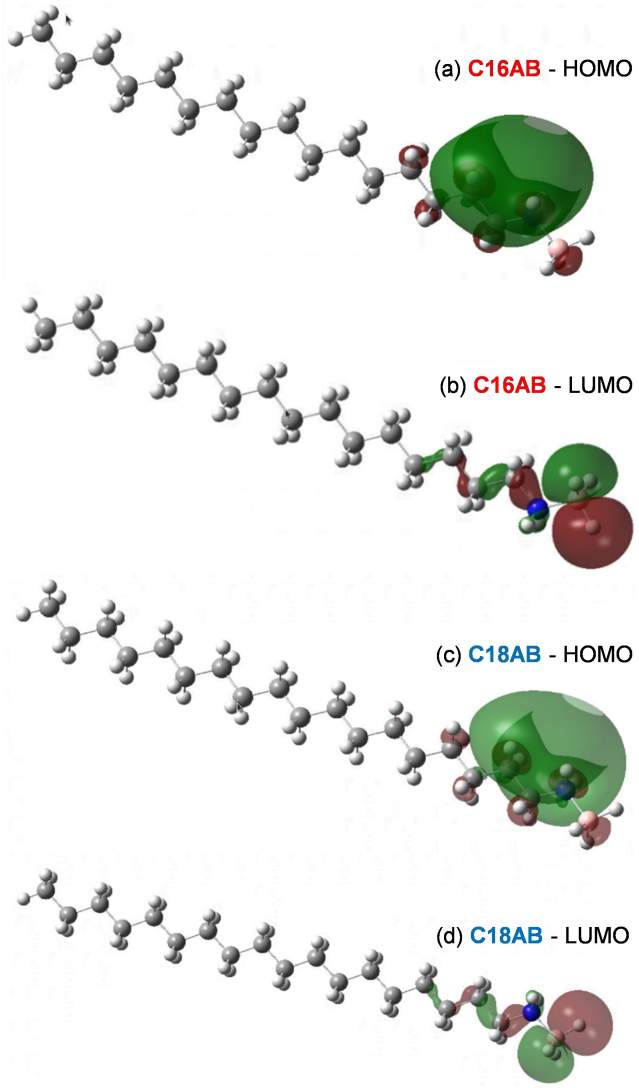

Figure 6. Contour plots (isosurface value: 0.02) of the HOMO and LUMO of the (a,b) C16AB and (c,d) C18AB molecules. Calculated by DFT at the B3LYP/6311G(2d,p) level.

Thermal analyses

C16AB and C18AB are stable when heated at $<100\,^{\circ}C$, and their melting is not concomitant with their decomposition. The onset temperatures of the melting event of C16AB and C18AB were thus determined by DSC (Figure S17). Melting is evidenced on heating by an endothermic signal and, on cooling, by crystallization (exothermic signal). The onset melting temperatures are 75.3 and 80 °C, respectively. They are higher than the melting points of the starting amines (44 °C for hexadecylamine and 51 °C for octadecylamine, respectively). This is indicative of additional intermolecular interactions, that is, of DHBs in the ABA.[18]

The onset melting temperatures of C16AB and C18AB can be compared to those of the lighter AABAs we reported previously.[16] They rather fit with the almost logarithmic evolution of the temperatures reported for C4AB to C14AB (Figure 7 and Figure S18).Occurrence of dihydrogen $H^{\delta+}\cdots H^{\delta-}$ bonds in these ABA make the melting points higher than those of the starting amines. The 'gain' is however less pronounced as the molecular weight of the alkyl chain increases.

For C4AB to C14AB, it was reported that the enthalpy of fusion increases by about 8.4 kJ mol^{-1} with the presence of two additional CH_2 groups.[16] For C16AB and C18AB, this trend is further confirmed (Figure S19). For instance, the enthalpy of fusion of C14AB is 48.1 kJ mol^{-1} versus 58.5 kJ mol^{-1} for C16AB. This is in line with the trend already reported for linear alkanes.[26] The larger the alkane (or alkyl) chain is, the stronger the intermolecular London forces are. The consequence is a concomitant increase of the melting points and enthalpies of fusion, as a function of the number of C atoms.

The thermal stability of C16AB was examined by TG analysis, and the evolving volatile decomposition products were analyzed by coupling TG analysis with microGC-MS and GC-MS. C16AB dehydrogenates from about 53 °C (Figure 8) and, below 250 °C, the dehydrogenation is featured by two events peaking at 126 and 200 °C. Pure H_2 is thus released below 200 °C and the weight loss at 200 °C is 1.4 wt%. This corresponds to the release of 3.6 H (1.8 equiv. H_2) over the 5 H of the NH_2BH_3 group. Above 275 °C and up to about 550 °C, C16AB significantly decomposes into carbonaceous fractions coming from the decomposition of the alkyl chain as obtained by GC-MS. Saturated and unsaturated C4 to C15 fractions (including some cyclic species like cyclohexene, 1-methylcyclohexene, cyclopentene, benzene and toluene) and methane (from TGA/microGC-MS) were detected, in good agreement with the cracking behavior of hexadecane.[27] The weight loss at 600 °C is as high as 90.9 wt%, whereas the content of B and N in C16AB corresponds to 9.7 wt%. This suggests that a small fraction of B and/or N of the NH_2BH_3

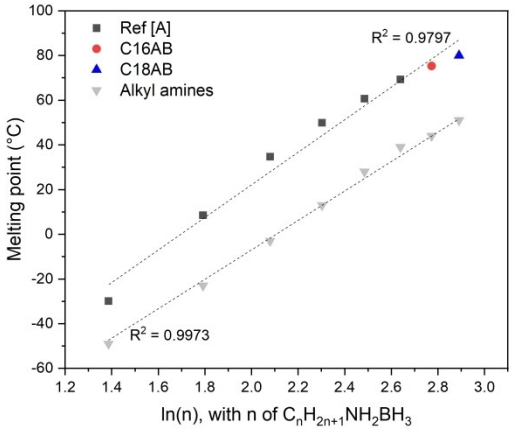

Figure 7. Evolution of the onset temperature of the endothermic signal shown in Figure S17 for C16AB and C18AB and in reference [16] (i.e. [A] in the legend) for C4AB to C14AB) as a function of the natural logarithm of n, the number of carbon atoms of $C_nH_{2n+1}NH_2BH_3$. The evolution of the melting points of the alkyl amines (as provided by the chemical supplier) is also shown for comparison.

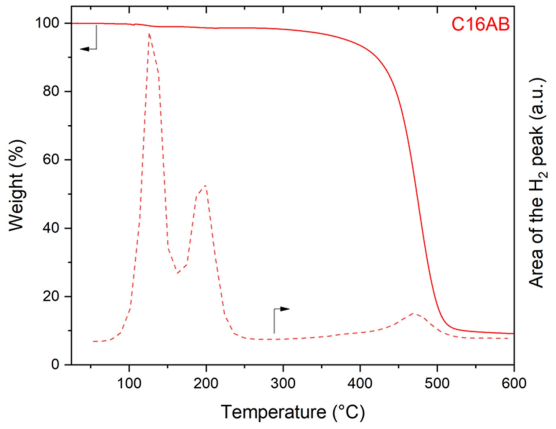

Figure 8. TG analysis of C16AB, coupled to microGC-MS in order to follow the evolution of H_2. The main weight loss between 275 and 550 °C are due to the release of hydrocarbon fragments as evidenced by TG analysis coupled GC-MS.

group have been lost as volatile products, and that the remaining solid is likely to be a boron nitride-based product.[28]

The thermal stability of C18AB (Figure S20) is comparable to that of C16AB. C18AB releases pure H_2 above 63 °C, and the dehydrogenation (1.1 wt%, that is, 1.55 equiv. H_2) shows two steps peaking at 140.3 and 204.1 °C. The main decomposition of C18AB occurs over the temperature range 300–600 °C and corresponds, as obtained by TG analysis coupled GC-MS, to the release of alkanes and alkenes from C4 to C17, as well as some cyclic compounds as those emitted from C16AB decomposition. The weight loss reaches 89.6 wt% at 600 °C, and this in line with the decomposition of the alkyl chain[29] into methane and C4 to C17 fragments. The remaining solid residue, 11.4 wt %, is likely to be mainly boron nitride-based.

Conclusion

The reaction of hexadecylamine or octadecylamine with borane dimethyl sulfide, in diethyl ether and under argon atmosphere, is exothermic (−59.4 and −69.7 kJ mol^{-1} respectively). The reaction results in the formation of the crystalline white solids C16AB and C18AB, as confirmed by the molecular and structural analyses.

C16AB and C18AB are isostructural (monoclinic, s.g. $P2_1/a$ (No. 14)) and their structural model shows antiparallel dimeric configurations for the NH_2BH_3 groups. This means that NH_2 of one molecule is facing BH_3 of another molecule; this takes place along the b axis (and the *bc* plane) with B-to-N distances between 4.05 and 4.3 Å. The DFT calculations (i. e. the Mulliken charges and the electrostatic potentials) indicate that the hydrogen atoms of NH_2BH_3 (for both C16AB and C18AB) are hydridic and protic. Such observations converge towards the existence and occurrence of DHBs, and suggest that the ABAs may be further exploited for molecular self-assembly and synthesis of advanced materials. Works are in progress with C16AB.

When heated up to < 100 °C, both C16AB and C18AB melt (onset temperatures of 75.3 and 80 °C, respectively). Above 100 °C and up to ca. 210 °C, they both dehydrogenate, releasing 1.4 and 1.1 wt% of pure H_2 respectively. This is pretty remarkable because ABAs generally decompose over this range of temperature. Such a result may open the way to lighter ABAs as potential hydrogen carriers.

Experimental Section

C16AB and C18AB were synthesized from commercial amines, both from Merck: hexadecylamine $CH_3(CH_2)_{15}NH_2$ (≥ 98 %; 241.46 g mol^{-1}; m.p. 43–45 °C) and octadecylamine $CH_3(CH_2)_{17}NH_2$ (≥ 99 %; 269.51 g mol^{-1}; m.p. 50–52 °C). A borane dimethyl sulfide $(CH_3)_2S{\cdot}BH_3$ complex solution (5.0 M in diethyl ether; 75.97 g mol^{-1}) was purchased from Merck and used as received. Anhydrous diethyl ether (≥ 99.7 %, from Merck) was used as solvent.

The AABAs were synthesized by substitution of the Lewis base $(CH_3)_2S$ of the borane dimethyl sulfide by an amine, in diethyl ether. Having dimethyl sulfide as the only reaction and a solvent like diethyl ether is convenient because both liquids have low boiling points (37.3 and 34.6 °C respectively), making their extraction easy. The AABAs were synthesized as follows. In an argon-filled glove box (MBraun M200B; $O_2 < 0.1$ ppm, $H_2O < 0.1$ ppm), 500 mg of an amine was dissolved in 8 mL of anhydrous diethyl ether, under stirring (500 rpm) for 1 h at ambient temperature. Thereafter, a slight excess of borane dimethyl sulfide complex (1.1 equiv.) was added dropwise to the amine solution; it is important to perform this step slowly as the reaction is exothermic. The mixture was kept under stirring for 24 h. Finally, the solution was transferred out of the glove box, and connected to a vacuum line to extract diethyl ether and dimethyl sulfide. Hexadecylamine borane $CH_3(CH_2)_{15}NH_2BH_3$ (C16AB; 255.29 g mol^{-1}) and octadecylamine borane $CH_3(CH_2)_{17}NH_2BH_3$ (C18AB; 283.34 g mol^{-1}) are white solids at 20–25 °C, which allowed performing the extraction step at ambient temperature for 2 h. Both solids were stored at −48 °C and under argon atmosphere.

The enthalpy of reaction for the AABAs was determined by Calvet calorimetry. The C80 calorimeter (from Setaram France) was used with reversal hermetic mixing cells (made of stainless steel, used for pressures up to 5 bar, and having two separated chambers). The cells were filled and closed in the glove box. The amine solution was poured in the 2.5 mL chamber and the borane solution was injected in the second chamber (2 mL capacity) with a syringe. We also used a reference cell that was kept empty. Both reference and sample cells were inserted in the calorimeter. The experiment was performed at 28 °C. The reactants were mixed by turning the calorimeter (and thus the cells) upside down several times with a rotational motion. That inversion process was stopped when the reaction peak reached its maximum. The heat flow was monitored against time, which allowed calculating the enthalpy of reaction.

Molecular analyses were performed using: Fourier-transform infrared spectroscopy (FTIR; IS50 Thermo Fisher Scientific; from 4000 to 650 cm^{-1}; 64 scans; resolution of 4 cm^{-1}); Raman spectroscopy (Horiba Jobin Yvon LabRAM 1B; laser Ar/Kr 100 mW 647.1 nm); ^{1}H nuclear magnetic resonance spectroscopy (^{1}HNMR; Bruker Avance-400 NMR; BBOF probe; CD_3CN; 5-mm NMR tube); ^{11}BNMR spectroscopy (Bruker AVANCE-400; probe head BBFO; CD_3CN; 5-mm tube;

128.378 MHz); solid-state ^{11}B magic angle spinning (MAS) NMR spectroscopy (^{11}B MASNMR; Varian VNMR4000; 128.378 MHz).

The structural models of C16AB and C18AB were obtained by Rietveld refinement from diffraction patterns collected at room temperature on a PANalytical X'PERT Pro multipurpose diffractometer (Cu-$K_{\alpha1}$ radiation, $\lambda = 1.54059$ Å, 45 kV and 40 mA) equipped with an X'Celerator detector and using Scherrer geometry. The acquisition time was about 10 h. The corresponding powders were loaded into 0.5 mm borosilicate glass capillary tubes in an argon-filled glove box (Jacomex PBOX; $O_2 < 1$ ppm, and $H_2O < 2$ ppm), and sealed in order to prevent the samples from moist air contamination. The unit cell parameters of the crystalline compounds were determined using DICVOL06,[30] and the diffraction patterns were indexed in the monoclinic system using the space group $P2_1/a$ (No. 14). In this space group, the number of asymmetric unit Z is assumed to be 4 for both. In this way, the average atomic volume for the carbon, boron and nitrogen atoms is close to 25.5 Å^3. This is in very good agreement with the Loganin criteria.[31] The crystal structures were solved using the software FOX.[32] The constitutive molecules have been considered flexible to reach the structural model without using any anti-bump. The as-obtained structural models were refined using the Rietveld method using the software Jana 2006.[33] Deposition Numbers 2204811 (for C16AB, hexadecylamine borane or $C_{16}H_{33}NH_2BH_3$) and 2204810 (for C18AB, octadecylamine borane or $C_{18}H_{35}NH_2BH_3$) contain the supplementary crystallographic data for this paper. These data are provided free of charge by the joint Cambridge Crystallographic Data Centre and Fachinformationszentrum Karlsruhe http://www.ccdc.cam.ac.uk/structures Access Structures service.

The melting points and enthalpies of fusion of the ABAs were determined by DSC (DSC 1 Mettler-Toledo). We used indium and mercury as standards to calibrate temperature, and indium and zinc to calibrate the melting enthalpy; this resulted in errors of $< 1\%$. We used sealable aluminum crucible (40 μL) to prevent the ABA from air contamination. The samples were prepared in the glove box, and the sealed crucibles were afterwards transferred into the DSC oven. The heating rate was 5 °C min^{-1}. The N_2 flow rate was 30 mL min^{-1}. We performed a full cycle consisting of a heating step and a cooling step. The thermal stability and decomposition of the ABA were studied by thermogravimetric (TG) analysis (TGA/DSC 2 Mettler Toledo; from 25 to 600 °C; heating of 5 °C min^{-1}; N_2 flow rate of 30 mL min^{-1}). The device was coupled to gas chromatography (GC) and mass spectrometry (MS) detector (7890B GC-5977A MSD Agilent Technologies). We actually used two types of couplings: TGA/microGC-MS (SRA Instrument) to follow H_2 (and to quantify it) and other small molecules like methane, and TGA/Storage-Interface/GC-MS for heavier volatile products. The samples (15 to 20 mg) were loaded into an aluminum crucible (100 μL) having a pierced lid and heated under pure nitrogen atmosphere.

The molecular structures of C16AB and C18AB were studied by density functional theory (DFT) calculations. A gas phase geometry optimization was performed using DFT/B3LYP method with the 6-311++G (2d, p) basis set available in Gaussian16. The optimized conformers were calculated at 298.15 K. The Mulliken charges, the electrostatic potentials, the HOMO and the LUMO were calculated.

Supporting Information Summary

The Supporting Information provides Figures S1 to S20 and Tables S1 to S3 that are cited throughout the article.

Acknowledgements

We thank the Agence Nationale de la Recherche (project 'REVERSIBLE' ANR-18-CE05-0032, and project 'A3' via LabEx CheMISyst ANR-10-LABX-05-01) and the Université de Montpellier (AAP Post-Doc UM 2016) for funding.

Conflict of Interest

The authors declare no conflict of interest.

Data Availability Statement

The data that support the findings of this study are available from the corresponding author upon reasonable request.

Keywords: alkylamine · amine borane adduct · boranes · dihydrogen bond

[1] a) B. Carboni, L. Monnier, *Tetrahedron* **1999**, *55*, 1197–1248; b) D. O. Reddy, *Chem. Rev. Lett.* **2020**, *3*, 184–191.
[2] U. B. Demirci, *Energies* **2020**, *13*, 3071.
[3] R. Kumar, A. Karkamkar, M. Bowden, T. Autrey, *Chem. Soc. Rev.* **2019**, *48*, 5350–5380.
[4] a) Y. Dai, X. Zhang, Y. Liu, H. Yu, J. Zhou, Q. Ye, Z. Huang, *J. Am. Chem. Soc.* **2022**, *144*, 8434–8438; b) G. Zhang, D. Morrison, G. Bao, H. Yu, C. W. Yoon, T. Song, J. Lee, A. T. Ung, Z. Huang, *Angew. Chem. Int. Ed.* **2021**, *60*, 11725–11729.
[5] a) B. S. Burnham, *Curr. Med. Chem.* **2005**, *12*, 1995–2010; b) A. Staubitz, A. P. M. Robertson, M. E. Sloan, I. Manners, *Chem. Rev.* **2010**, *110*, 4023–4078.
[6] a) L. Capaldo, T. Noël, D. Ravelli, *Chem. Catal.* **2022**, *2(5)*, 957–966; b) P. V. Ramachandran, H. J. Hamann, S. Mishra, *ACS Omega* **2022**, *7*, 14377–14389; c) Y. Zhang, Y. Liao, P. Liu, Y. Ran, X. Liu, *Org. Biomol. Chem.* **2022**, *20*, 3550–3557.
[7] M. Birepinte, V. Liautard, L. Chabaud, M. Pucheault, *Org. Lett.* **2020**, *22*, 2838–2843.
[8] a) V. Liautard, M. Delgado, B. Colin, L. Chabaud, G. Michaud, M. Pucheault, *Chem. Commun.* **2022**, *58*, 2124–2127; b) A. Gilbert, P. Langowski, M. Delgado, L. Chabaud, M. Pucheault, J. F. Paquin, *Beilstein J. Org. Chem.* **2020**, *16*, 3069–3077.
[9] a) C. Frabitore, J. Lépeule, B. Towey, T. Livinghouse, W. C. Robinson, *Int. J. Rapid Commun. Synth. Org. Chem.* **2021**, *52*, 185–189; b) S. Gurram, G. Srivastava, V. Badve, V. Nandre, S. Gundu, P. Doshi, *Appl. Biochem. Biotechnol.* **2022**, *194*, 827–847.
[10] S. Lau, D. Gasperini, R. L. Webster, *Angew. Chem. Int. Ed.* **2021**, *60*, 14272–14294.
[11] a) M. Delarmelina, J. W. de M. Carneiro, C. R. A. Catlow, M. Bühl, *Catal. Commun.* **2022**, *162*, 106385; b) A. V. Bhujbal, T. A. Gokhale, B. M. Bhanage, *Waste Biomass Valorization* **2022**, *13*, 443–451.
[12] D. Han, F. Anne, M. Trose, T. Beweries, *Coord. Chem. Rev.* **2019**, *380*, 260–286.
[13] H. Sheng, X. Huang, Y. Ji, Z. Zhao, W. Hu, J. Chen, Z. Ji, X. Wang, H. Liu, *Fuel* **2022**, *321*, 124098.
[14] G. Bourbon, R. Leroy, C. Machado-Rodrigues, G. Massiot, *Phytochem. Lett.* **2022**, *48*, 40–42.
[15] a) R. H. Crabtree, P. E. M. Siegbahn, O. Eisenstein, A. L. Rheingold, T. F. Koetzle, *Acc. Chem. Res.* **1996**, *29*, 348–354; b) N. V. Belkova, E. S. Shubina, L. M. Epstein, *Acc. Chem. Res.* **2005**, *38*, 624–631.
[16] a) K. Turani-I-Belloto, M. J. Valero-Pedraza, R. Chiriac, F. Toche, D. Granier, D. Cot, E. Petit, P. G. Yot, J. G. Alauzun, U. B. Demirci, *ChemistrySelect* **2021**, *6*, 9853–9860; b) A. Theodoratou, K. Turani-I-Belloto, E. Petit, S. Dourdain, J. G. Alauzun, U. B. Demirci, *J. Mol. Struct.* **2022**, *1248*, 131484.
[17] a) T. S. Khasanshin, A. P. Shchamialiou, O. G. Poddubski, *Int. J. Thermophys.* **2003**, *24*, 1277–1289; b) E. W. Lemmon, M. L. Huber, *Energy Fuels*

2004, *18*, 960–967; c) J. Smolke, F. Carbone, F. N. Egolfopoulos, H. Wang, *Combust. Flame* **2018**, *190*, 65–73.
[18] X. Chen, J. C. Zhao, S. G. Shore, *Acc. Chem. Res.* **2013**, *46*, 2666–2675.
[19] Q. Zhao, J. Li, E. J. M. Hamilton, X. Chen, *J. Organomet. Chem.* **2015**, *798*, 24–29.
[20] M. Paskevicius, L. H. Jepsen, P. Schouwink, R. Černý, D. B. Ravnsbæk, Y. Filinchuk, M. Dornheim, F. Besenbacher, T. R. Jensen, *Chem. Soc. Rev.* **2017**, *46*, 1565–1634.
[21] a) T. E. Reich, K. T. Jackson, S. Li, P. Jena, H. M. El-Kaderi, *J. Mater. Chem.* **2011**, *21*, 10629–10632; b) N. A. Riensch, A. Deniz, S. Kühl, L. Müller, A. Adams, A. Pich, H. Helten, *Polym. Chem.* **2017**, *8*, 5264–5268; c) C. A. de Albuquerque Pinheiro, C. Roiland, P. Jehan, G. Alcaraz, *Angew. Chem. Int. Ed.* **2018**, *57*, 1519–1522; *Angew. Chem.* **2018**, *130*, 1535–1538.
[22] a) J. R. Durig, N. E. Lindsay, T. J. Hizer, J. D. Odom, *J. Mol. Struct.* **1988**, *189*, 257–277; b) F. Leardini, M. J. Valero-Pedraza, E. Perez-Mayoral, R. Cantelli, M. A. Banares, *J. Phys. Chem. C* **2014**, *118*, 17221–17230.
[23] G. R. Eaton, *J. Chem. Educ.* **1969**, *46*, 547–556.
[24] B. Roy, U. Pal, A. Bishnoi, L. A. O'Dell, P. Sharma, *Chem. Commun.* **2021**, *57*, 1887–1890.
[25] T. Kobayashi, S. Gupta, M. A. Caporini, V. K. Pecharsky, M. Pruski, *J. Phys. Chem. C* **2014**, *118*, 19548–19555.
[26] a) D. L. Dorset, H. L. Strauss, R. G. Snyder, *J. Phys. Chem.* **1991**, *95*, 938–940; b) A. D. Bond, *New J. Chem.* **2004**, *28*, 104–114.
[27] A. K. Burnham, H. R. Gregg, R. L. Ward, K. G. Knauss, S. A. Copenhaver, J. G. Reynolds, R. Sanborn, *Geochim. Cosmochim. Acta* **1997**, *61*, 3725–3737.
[28] F. Guilhon, B. Bonnetot, D. Cornu, H. Mongeot, *Polyhedron* **1996**, *15*, 851–859.
[29] H. Zhang, A. Geng, Y. Xiong, J. Liu, J. Liu, *Geochem. J.* **2008**, *42*, 403–412.
[30] A. Boultif, D. Louër, *J. Appl. Crystallogr.* **1991**, *24*, 987–993.
[31] C. Giacovazzo, *Phasing in Crystallography: A Modern Perspective*, IUCr Texts on Crystallography, International Union of Crystallography Oxford University Press, **2013**, No. 20.
[32] V. Favre-Nicolin, R. Cerny, *J. Appl. Crystallogr.* **2002**, *35*, 734–743.
[33] V. Petricek, M. Dusek, L. Palatinus, *Z. Kristallogr.* **2014**, *229*, 345–352.

Submitted: September 9, 2022
Accepted: October 24, 2022